ACS OMEGA

http://pubs.acs.org/journal/acsodf

Article

# Effect of Pressure on the Superconducting Transition Temperature and Physical Properties of $CaPd_2P_2$: A DFT Investigation

Jakiul Islam,* Nahida Farjana, Md Didarul Islam, Shamaita Shabnam, and Md Afjalur Rahman

Cite This: *ACS Omega* 2022, 7, 21528−21536

Read Online

ACCESS | Metrics & More | Article Recommendations

**ABSTRACT:** $CaPd_2P_2$ is a recently reported superconducting material belonging to the well-known $ThCr_2Si_2$-type family. First-principles density functional theory calculations have been carried out to investigate the structural, mechanical, thermophysical, optical, electronic, and superconducting properties of the $CaPd_2P_2$ compound under pressure. To the best of our knowledge, this is the first theoretical approach to studying the pressure effect on the fundamental physical and superconducting properties of $CaPd_2P_2$. It is mechanically stable under the studied pressures. The applied hydrostatic pressure reveals a noticeable impact on elastic moduli of $CaPd_2P_2$. It exhibits ductile nature under the studied pressure. Significant anisotropic behavior of the compound is revealed with/without pressure. The study of melting temperature shows that the compound has a higher melting temperature, which increases with the increasing applied pressure. The investigation of the electronic properties strongly supports the optical function analysis. The reflectivity as well as the absorption spectra shifts to higher energy with the increasing applied pressure. The pressure-dependent behavior of the superconducting transition temperature, $T_c$, is revealed with a pressure-induced increasing trend in Debye temperature.

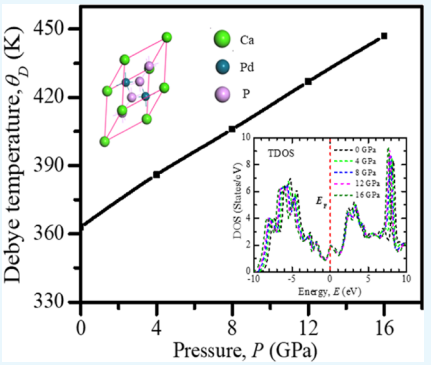


## 1. INTRODUCTION

The world technology is being developed every day through advanced levels of research activities to make human life easier. Superconductivity is one of the most fascinating discoveries to make the real world faster, but it is still puzzling for the research community even more than 100 years after its invention.[1] Most of the superconductors exhibit low-temperature superconductivity. Therefore, the practical application of superconducting materials is difficult. Considering this, researchers in the field of superconductivity have been developing materials with room-temperature superconductivity. In recent years, several research works have been performed to achieve room-temperature superconductivity.[2−18] Most of these researches were performed under high pressure.[2−12] In 2020, Snider et al.[5] claimed to have achieved room-temperature superconductivity in a carbonaceous sulfur hydride under high pressure (267 ± 10 GPa), providing a ray of hope. Although their research raises several questions,[19−23] it has provided a new thrust to the researchers in this field to search for new materials with high-temperature superconductivity. In 2020, Blawat et al. observed superconductivity at the transition temperatures, $T_c$, of nearly 1.0 and ∼0.7 K in $CaPd_2P_2$ and $SrPd_2P_2$ compounds, respectively.[24] In 2021, Islam and Hossain theoretically proved low-temperature superconductivity in $CaPd_2P_2$ and $SrPd_2P_2$.[25] Both of these are one of the 700 members of the $ThCr_2Si_2$-type materials (also called the 122 family) and exhibit fascinating chemical and physical properties.[26] The $ThCr_2Si_2$-structure was introduced in 1965 by Ban and Sikirica.[27] The $APd_2P_2$ class was first reported in 1983.[28] The $ThCr_2Si_2$-type $AT_2X_2$ (where A = lanthanide or alkaline earth elements; T = transition metals; X = P, Se, Si, Ge, or As) crystals have gained massive attention of the research community due to their diverse properties such as superconductivity at low $T_c$[29,30] and high $T_c$,[31,32] pressure-induced superconductivity,[33−36] superconductivity generated by doping,[37−39] and magnetic and anti-ferromagnetic characteristics.[40,41] In 2021, Parvin and Naqib exhibited the pressure effect on low-temperature pnictide superconductor $NaSn_2P_2$.[42] They predicted the pressure-dependent characteristics of $T_c$ with a pressure-induced variation in the Debye temperature.

The knowledge of mechanical properties is required to know the suitability of a compound for application in a particular device. The study of the thermophysical properties, which reveals the behavior of a compound at different temperatures and pressures, is also very important. In addition, an investigation of the optical properties provides valuable information that can support to design of optoelectronic devices. The study of the electronic band structure and the density of states at the Fermi level is particularly important for

Received: February 23, 2022
Accepted: May 30, 2022
Published: June 13, 2022

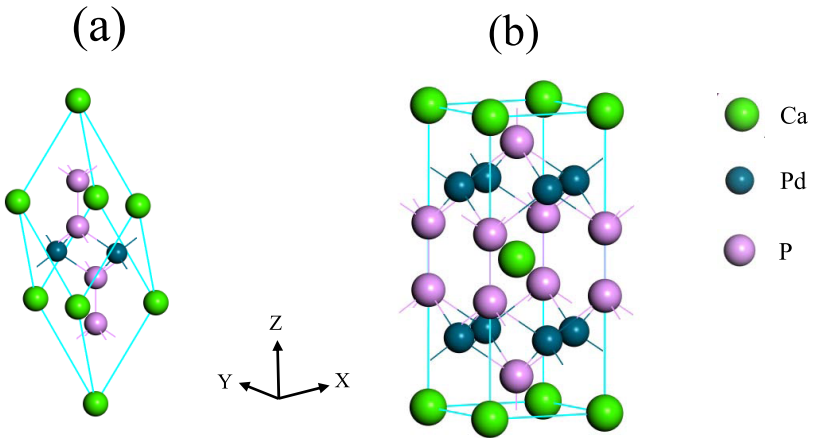


**Figure 1.** Constructed crystal of the $CaPd_2P_2$ compound: (a) primitive cell and (b) conventional unit cell.

gaining useful information about the parameters responsible for making a material a superconductor. The application of hydrostatic pressure is an efficient and environmental-friendly thermodynamic approach for altering the physical properties of materials. The elastic constant provides valuable information about mechanical stability, bonding strength, and stiffness of solid materials. Therefore, the pressure-dependent behavior of elastic constants is quite important to investigate. The pressure-induced variation in the elastic anisotropy of a crystal is required to gather information about any possible microcracks/defects that develop in a crystal with applied pressure.

To the best of our knowledge, none of the fundamental physical properties mentioned in the above section has been studied yet in detail for the recently reported $ThCr_2Si_2$-type $CaPd_2P_2$ compound. Therefore, the present approach deals with a detailed theoretical investigation of the structural, mechanical, electronic, optical, thermophysical, and superconducting properties of $CaPd_2P_2$ under pressure using density functional theory (DFT)-based Cambridge serial total energy package (CASTEP) code. The comprehensive calculations and new findings displayed in this research provide valuable insight into the probable applications of $CaPd_2P_2$ in the future. The authors believe that this study would be useful enough for designing as well as carrying out research on superconducting materials under pressure.

## 2. COMPUTATIONAL METHODS

In this investigation, CASTEP computer code[43] based on DFT[44,45] was used for the geometry optimization and investigation of properties. A generalized gradient approximation (GGA) along with the Perdew–Burke–Ernzerhof (PBE) method[46] was employed for this study. Vanderbilt[47] ultrasoft pseudopotential was used for the description of the electron–ion interaction. The pseudo-atomic calculations were performed by taking only valance electrons. The *k*-points $16 \times 16 \times 7$ along with the cutoff energy 700 eV were chosen for this DFT investigation. The Monkhorst–Pack schemes[48] were used for the Brillouin zone sampling of *k*-points. The Broyden–Fletcher–Goldfarb–Shanno (BFGS) technique[49] was inserted to ensure the optimized structure of the $CaPd_2P_2$ compound. The elastic constants of $CaPd_2P_2$ were computed using the "stress–strain" theory.[50] The strain amplitude was fixed to 0.003. The convergence criteria were settled as follows: energy, maximum displacement, maximum stress, and maximum force; and $10^{-5}$ eV/atom, 0.001 Å, 0.05 GPa, and 0.03 eV/Å.

## 3. RESULTS AND DISCUSSION

**3.1. Structural Properties.** The $CaPd_2P_2$ compound possesses a tetragonal structure along with the space group *I*4/*mmm* (no.139) of the renowned $ThCr_2Si_2$-type family. The Ca, Pd, and P atoms occupy 2a (0, 0, 0), 4d (0, 0.5, 0.25), and 4e (0, 0, 0.3882) Wyckoff sites, respectively.[24] Figure 1 depicts the primitive cell and conventional unit cell of $CaPd_2P_2$.

The optimized lattice parameters are listed in Table 1 along with available experimental and theoretical values.[24,25] At 0 GPa, the DFT-optimized lattice parameters are well in accordance with the experimental results.[24]

**Table 1. Calculated Lattice Parameters *a* and *c* and the Unit Cell Volume, *V*, of $CaPd_2P_2$ under Different Applied Pressures**

| *P* (GPa) | *a* (Å) | *c* (Å) | *V* (Å$^3$) | ref |
|---|---|---|---|---|
| 0 (exp.) | 4.137 | 9.649 | 165.13 | 24 |
| 0 (GGA) | 4.036 | 10.203 | 166.20 | 25 |
| 0 | 4.037 | 10.201 | 166.25 | this |
| 4 | 3.986 | 10.119 | 160.77 | this |
| 8 | 3.944 | 10.049 | 156.31 | this |
| 12 | 3.906 | 9.991 | 152.43 | this |
| 16 | 3.874 | 9.931 | 149.04 | this |

The decreasing trend in lattice parameters is observed with the increase in pressure, which infers that the space among the atoms is reduced. As a consequence, the repulsive effect between the atoms increases, which benefits the stiffness of crystal compression under pressure. To the best of our knowledge, this is the first theoretical approach to investigate the pressure effect on $CaPd_2P_2$; as a result, it was not possible to make a comparative analysis of this study with other investigations.

**3.2. Mechanical Properties.** To obtain information on the mechanical stability, bonding nature, and stiffness of solid materials, elastic constants are a key criterion. Tetragonal structures like that of $CaPd_2P_2$ consist of six different elastic constants, $C_{11}$, $C_{12}$, $C_{13}$, $C_{33}$, $C_{44}$, and $C_{66}$, which are tabulated in Table 2. The elastic constants $C_{11}$ and $C_{33}$ are related to the uniaxial stress (resistance to linear compression) and the other four reflect the shear-dominated responses (connected with the elasticity in shape). From Table 2, it can be noticed that the values of $C_{11}$ and $C_{33}$ are noticeably higher than those of other elastic constants under the studied pressures, which indicates that the $CaPd_2P_2$ compound cannot be compressed easily under


https://doi.org/10.1021/acsomega.2c01088
ACS Omega 2022, 7, 21528−21536

Table 2. Calculated Elastic Constants $C_{ij}$ (in GPa) of the $CaPd_2P_2$ Compound

| $P$ (GPa) | $C_{11}$ | $C_{12}$ | $C_{13}$ | $C_{33}$ | $C_{44}$ | $C_{66}$ | ref |
|---|---|---|---|---|---|---|---|
| 0 (GGA) | 161.61 | 84.66 | 80.55 | 218.66 | 57.15 | 39.11 | 25 |
| 0 | 161.65 | 87.72 | 80.52 | 219.99 | 57.10 | 39.67 | this |
| 4 | 186.70 | 103.50 | 89.40 | 232.59 | 64.56 | 46.45 | this |
| 8 | 206.49 | 117.20 | 113.77 | 265.85 | 71.06 | 61.03 | this |
| 12 | 229.61 | 135.45 | 128.15 | 312.48 | 74.80 | 75.91 | this |
| 16 | 254.16 | 152.82 | 140.53 | 331.30 | 84.03 | 86.47 | this |

Table 3. Calculated Values of Bulk Modulus, $B$ (GPa), Shear Modulus, $G$ (GPa), Young's Modulus, $E$ (GPa), Pugh's Ratio, $B/G$, Poisson's Ratio, $\nu$, and Universal Anisotropy, $A^U$, of $CaPd_2P_2$

| $P$ (GPa) | $B_V$ | $B_R$ | $B$ | $G_V$ | $G_R$ | $G$ | $E$ | $B/G$ | $\nu$ | $A^U$ | ref |
|---|---|---|---|---|---|---|---|---|---|---|---|
| 0 | 114.82 | 113.10 | 113.96 | 50.42 | 48.36 | 49.39 | 129.47 | 2.31 | 0.31 | 0.23 | 25 |
| 0 | 115.65 | 114.06 | 114.85 | 50.41 | 48.15 | 49.28 | 129.34 | 2.33 | 0.31 | 0.25 | this |
| 4 | 130.06 | 129.50 | 129.78 | 56.69 | 54.53 | 55.61 | 145.98 | 2.33 | 0.31 | 0.20 | this |
| 8 | 152.04 | 150.30 | 151.17 | 62.90 | 60.91 | 61.90 | 163.40 | 2.44 | 0.32 | 0.18 | this |
| 12 | 172.80 | 170.14 | 171.47 | 70.43 | 67.65 | 69.04 | 182.61 | 2.48 | 0.32 | 0.22 | this |
| 16 | 189.71 | 187.87 | 188.79 | 77.95 | 74.58 | 76.26 | 201.64 | 2.48 | 0.32 | 0.24 | this |

uniaxial stress. The mechanical stability criteria[51] comprising these constants without pressure conditions are as follows.

$$C_{11} > 0,\ C_{33} > 0,\ C_{44} > 0,\ C_{66} > 0$$
$$[C_{11} - C_{12} > 0,\ C_{11} + C_{33} - 2C_{13} > 0]$$
$$2(C_{11} + C_{12}) + C_{33} + 4C_{13} > 0 \quad (1)$$

$CaPd_2P_2$ satisfies the above stability conditions, which was also observed in an earlier study at 0 GPa.[25] Moreover, $CaPd_2P_2$ is also dynamically stable, as observed in a previous study.[24] As this is the first theoretical approach to study the mechanical properties under pressure, mechanical stability is required to be observed under pressure. The mechanical stability of the tetragonal crystal under pressure can be observed from the following conditions[52−54]

$$C_{44} - P > 0,\ C_{66} - P > 0$$
$$[C_{11} - C_{12} - 2P > 0,\ ]$$
$$(C_{33} - P)(C_{11} + C_{12}) - 2(C_{13} + P)^2 > 0 \quad (2)$$

From Table 2, it can be observed that $CaPd_2P_2$ satisfies the above stability conditions under the studied pressure. The values in Table 3 are found using the formulae from the Voigt−Reuss−Hill (VRH) averaging schemes.[55−57] The tabulated data includes bulk modulus ($B$), shear modulus ($G$), Young's modulus ($E$), Pugh's ratio ($B/G$), and Poisson's ratio ($\nu$), and universal anisotropy indices $A^U$. In Table 3, $B_V$ and $B_R$ denote the Voigt and Reuss approximated bulk moduli, respectively. The shear moduli approximated by Voigt and Reuss are denoted as $G_V$ and $G_R$, respectively.

It is known that a lower (higher) value of the bulk modulus and other elastic moduli is indicative of the soft (hard) nature of the crystal.[58−60] From Table 3, we can conclude that the softness of $CaPd_2P_2$ decreases with the increase in pressure, which is revealed by the gradual increase in $B$ values. Therefore, it is more difficult to change the volume of the compound under higher pressures.

Pugh's ratio and Poisson's ratio are useful indicators of the ductility/brittleness of a solid. The $B/G$ value lower than 1.75 is indicative of a brittle behavior, while the value higher than 1.75 indicates a ductile nature.[25,61] Similarly, the critical value of $\nu$ is 0.26, higher than the critical value indicating ductility and those lower than the critical value indicating brittleness.[25,62] Since ductile materials are convenient for fabricating devices, it is important to understand their ductility/brittleness. According to the values tabulated in Table 3, the $B/G$ and $\nu$ values are all above 1.75 and 0.26, respectively, thus indicating the ductile behavior of $CaPd_2P_2$ under the studied pressure. The value of $\nu$ can also be an indicator of the nature of interatomic forces present in bonding within solids.[63] Materials with atomic bonding dominated by the central force interaction have $\nu$ within the range of 0.25−0.50. In this study, the $\nu$ is within the domain of 0.25−0.50, indicating the dominance of a central force interaction in the atomic bonding of the crystal structure.

The shear modulus ($G$) is an indicator of shear resistance. At all pressures, $G$ is less than $B$, which implies that shape-deforming stress should be used to control the mechanical failure mode of $CaPd_2P_2$ instead of the volume-changing stress. Young's modulus ($E$) is defined as the resistance of a solid to compressive or tensile stress. The increasing values of $E$ with the increasing pressure indicate that the ability to withstand tensile stress is increased with the increase in applied pressure.

Elastic anisotropy is a highly significant parameter of the crystalline solids. The study of anisotropy is necessarily important due to the different bonding natures along different crystallographic directions. This provides information about the possibility to generate microfractures in solid. The universal anisotropic characteristic, $A^U$, is theoretically determined by an equation given elsewhere.[25,64] If the $A^U$ value is equal to zero, then the crystal is isotropic; any deviation signifies anisotropic nature. $CaPd_2P_2$ exhibits significant anisotropic nature under the studied pressure, which suggests that the mechanical properties of the compound depend on the direction.

### 3.3. Debye Temperature and Melting Temperature.

The Debye temperature, $\theta_D$, is a very significant thermophysical criterion of solid that indicates the highest frequency mode of vibration. It is a boundary between the low- and high-temperature regions of solid. When the temperature of the solid is higher than $\theta_D$ (i.e., $T > \theta_D$), the vibration mode is considered to have $k_BT$ energy and in the case of $T < \theta_D$, the vibration mode is expected to be at rest.[65] The low-temperature vibration is a result of acoustic vibration. The $\theta_D$ is related to different thermodynamic parameters such as the thermal expansion of solids, phonons, thermal conductivity, specific


https://doi.org/10.1021/acsomega.2c01088
ACS Omega 2022, 7, 21528−21536

**Table 4. Calculated Values of Density, $\rho$, Transverse Sound Velocity, $v_t$, Longitudinal Sound Velocity, $v_l$, Mean Sound Velocity, $v_m$, Debye Temperature, $\theta_D$, and Melting Temperature, $T_m$, of the $CaPd_2P_2$ Compound**

| pressure (GPa) | $\rho$ (g/cc) | $v_l$ (m/s) | $v_t$ (m/s) | $v_m$ (m/s) | $\theta_D$ (K) | $T_m$ | ref |
|---|---|---|---|---|---|---|---|
| 0 | 6.29 | 5346.70 | 2802.17 | 3134.22 | 365 | 1166 | 25 |
| 0 | 6.29 | 5357.73 | 2779.05 | 3110.49 | 363 | 1165 | this |
| 4 | 6.50 | 5601.19 | 2924.95 | 3272.34 | 386 | 1260 | this |
| 8 | 6.69 | 5910.43 | 3041.81 | 3406.31 | 406 | 1369 | this |
| 12 | 6.86 | 6197.94 | 3172.40 | 3553.77 | 427 | 1511 | this |
| 16 | 7.02 | 6432.53 | 3295.94 | 3691.92 | 447 | 1613 | this |

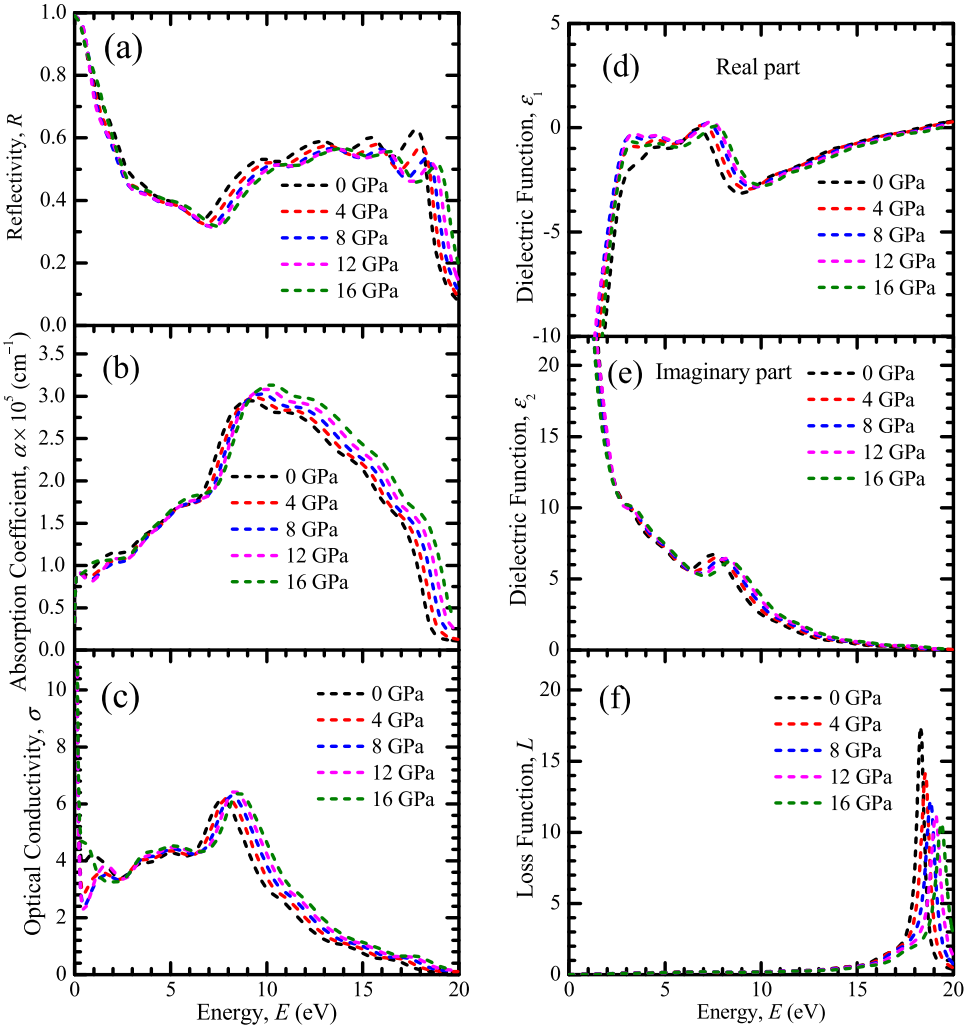


**Figure 2.** Optical functions of (a) reflectivity, (b) optical absorption, (c) optical conductivity, (d) real part of dielectric function, (e) imaginary part of dielectric function, and (f) loss function of $CaPd_2P_2$ under different pressures.

heat, and melting point. The superconducting transition temperature, $T_c$, is also largely associated with $\theta_D$. As a result, the variation in the $\theta_D$ value with the applied pressure is highly significant for $T_c$. There are several approaches for evaluating $\theta_D$. In the present research, $\theta_D$ is estimated using elastic moduli, which is considered one of the standard ways.[66] The average sound velocity ($v_m$), transverse sound velocity ($v_t$), and longitudinal sound velocity ($v_l$) are related to the estimation of $\theta_D$ via the following equations[67−70]

$$\theta_D = \frac{h}{k_B}\left[\frac{3n}{4\pi}\left(\frac{N_A\rho}{M}\right)\right]^{1/3} v_m \quad (3)$$

$$v_m = \left[\frac{1}{3}\left(\frac{2}{v_t^3} + \frac{1}{v_l^3}\right)\right]^{-1/3} \quad (4)$$

$$v_l = \left(\frac{B + \frac{4}{3}G}{\rho}\right)^{1/2} \quad (5)$$

$$v_t = \left(\frac{G}{\rho}\right)^{1/2} \quad (6)$$

where $k_B$, $h$, $N_A$, $M$, $\rho$, and $n$ indicate the Boltzmann constant, the Planck constant, Avogadro's number, the molecular mass, the



https://doi.org/10.1021/acsomega.2c01088
ACS Omega 2022, 7, 21528−21536

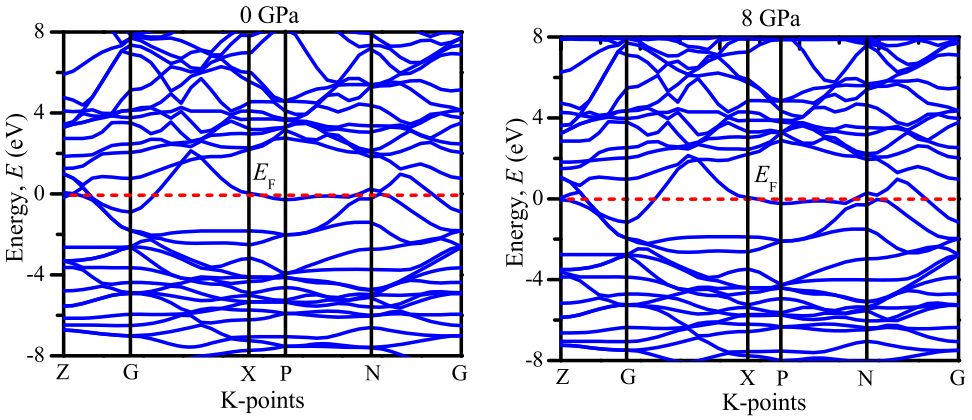


**Figure 3.** Calculated electronic band structure of $CaPd_2P_2$ at 0 and 8 GPa pressure.

density, and the number of atoms in the unit cell, respectively. $\theta_D$ of $CaPd_2P_2$ is calculated up to 16 GPa, with a step of 4 GPa. The computed values of $\rho$, $v_t$, $v_l$, $v_m$, and $\theta_D$ are tabulated in Table 4. At 0 GPa, the theoretically estimated value of $\theta_D$ is higher in comparison with the experimental result.[24] Precise measurement of $\theta_D$ is difficult; in a number of cases, experimental and theoretical values of $\theta_D$ show a larger variation.[71,72] The effect of pressure on $\theta_D$ is clearly observed in Table 4. It is exhibited that $\theta_D$ increases with the increasing applied pressure. This is the expected behavior of solid because the crystal becomes stiffer under pressure. Consequently, $\theta_D$ shows increasing affinity with the increasing applied pressure.

The transformation of the solid phase into the liquid phase at a certain temperature is indicated as the melting temperature, $T_m$. This is another crucial thermophysical criterion of the application of a material at a particular temperature and also reflects the strength of the bond in solids. $T_m$ is evaluated using elastic constants via the following equation[73]

$$T_m = 354 + 4.5\frac{2C_{11} + C_{33}}{3} \quad (7)$$

$T_m$ of $CaPd_2P_2$ increases with the increase in applied pressure as displayed in Table 4, which is the result of the increasing trend in $C_{11}$ and $C_{33}$ (these two elastic constants are related to uniaxial stress) with the increase in applied pressure (Table 2). The increasing affinity of $T_m$ benefits the bond strength with the increase in applied pressure.

**3.4. Optical Properties.** The optical properties of material provide significant information, particularly for the application of optoelectronic devices. It is essential to study the material response to the incident electromagnetic radiation. Therefore, the fundamental optical properties such as reflectivity ($R$), optical absorption ($\alpha$), optical conductivity ($\sigma$), real ($\varepsilon_1$), and imaginary ($\varepsilon_2$) parts of dielectric functions as a function of photon energy are calculated in this study. For metallic compounds, plasma energy (between 2 and 10 eV) is required for analyzing the optical functions.[25] In this study, 6 eV of plasma energy was used to study the optical functions of the $CaPd_2P_2$ compound. The optical functions are analyzed along the [100] polarization direction.

The reflectivity profile offers a crucial idea about the appropriateness of a material as a reflector. Figure 2a represents the pressure-induced reflectivity spectra of $CaPd_2P_2$ up to 20 eV of photon energy. Maximum reflectivity is observed at zero photon energy, which reduces sharply with the increasing photon energy, reaches a minimum near 6.5 eV. The reflectivity further increases above 6.5 eV and becomes flat over a wide range in the ultraviolet (UV) region of 9−18 eV. This result suggests that $CaPd_2P_2$ can be used as a prominent reflector in a wide range of UV radiation. It is also noticed from the analysis that the reflectivity does not change to a greater extent with the applied pressure. However, the reflectivity spectra shift to the higher energy above 18 eV with the increasing applied pressure.

The absorption coefficient measures the attenuation of light intensity while passing through a material. A lower absorption coefficient means more radiation can pass through the material and vice versa. The absorption profile of $CaPd_2P_2$ is depicted in Figure 2b. The optical absorption starts to increase with the increasing photon energy and reaches a maximum at ∼9.0 to 10 eV (upper limit of plasma energy) and then falls gradually. It is interesting to notice that up to 10 eV of photon energy, there is no significant effect of external pressure on absorption, while at photon energy >10 eV, the absorption spectra shift to the higher energy with the increasing external pressure.

The real part of the optical conductivity of the $CaPd_2P_2$ compound under high hydrostatic pressure is illustrated in Figure 2c for up to 20 eV of photon energy. It is noticed that the optical conductivity is maximum at the zero photon energy and then decreases sharply with the start of absorption of photons of low energies, and then further increases and reaches a peak position at ∼8 eV and then again decreases gradually with the increase in incident energy. These behaviors strongly support the metallic entity of $CaPd_2P_2$, which justifies the analysis of electronic properties and absorption profile. It is noticed that the conductivity spectra shift to the higher energy with the increasing applied pressures, which is also observed in the optical absorption profile.

Figure 2d,e displays the real and imaginary parts of the dielectric functions, respectively, at different external pressures of up to 20 eV of photon energy. Figure 2d displays that the real part of the dielectric function displays $\varepsilon_1 < 0$ at zero photon energy as well as low photon energies, indicating the metallic nature of $CaPd_2P_2$. Previous studies by Islam[25] and Hossain showed that the $\varepsilon_1$ value reaches unity and the $\varepsilon_2$ value reaches approximately zero under higher photon energy, suggesting that $CaPd_2P_2$ is expected to appear as a transparent material in the high energy region. The applied hydrostatic pressure on $CaPd_2P_2$ does not influence its dielectric functions significantly. The imaginary part of the dielectric function is largely associated with the optical absorption profile.[25] As the optical absorption profile does not change significantly with the applied pressure, dielectric functions remain almost invariant with pressure.


https://doi.org/10.1021/acsomega.2c01088
ACS Omega 2022, 7, 21528−21536

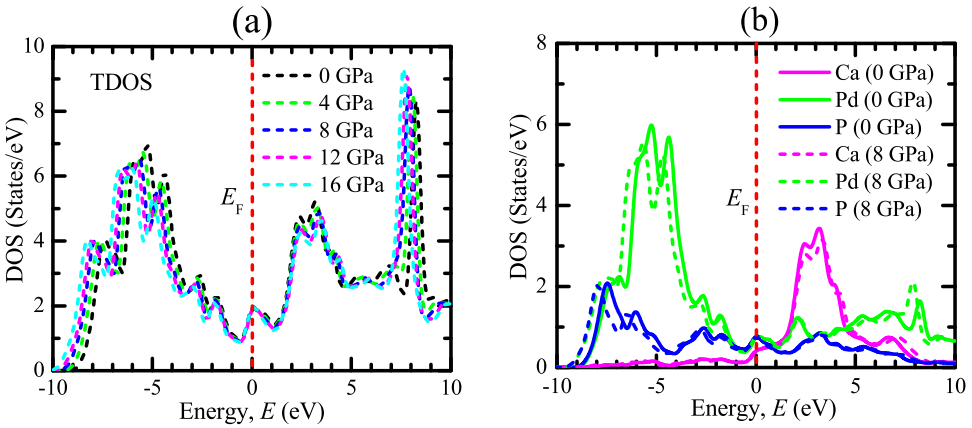


**Figure 4.** Calculated (a) TDOS of the $CaPd_2P_2$ compound at 0, 4, 8, 12, and 16 GPa pressure and (b) DOS of Ca, Pd, and P atoms in the $CaPd_2P_2$ compound at 0 and 8 GPa pressure.

The loss function measures the loss of energy of an electron traversing through a material. At 0 GPa, the loss function exhibits a sharp peak near about 18 eV of photon energy. The optical behavior of a metallic system changes to a dielectric-like response above the plasma energy.[42] The peak of loss function shifts to the higher energy with the increasing applied pressure, which also supports the analysis of optical absorption and reflectivity spectra. After certain photon energy (~18 eV for the $CaPd_2P_2$ compound), the peak shifts in the direction of higher energies with the increase in applied pressure such that the number of effective electrons participating in the intraband as well as the interband transitions are reduced.[74]

**3.5. Electronic Properties.** The electronic band structures of solids provide significant information about their physical properties, which can be determined by the conduction and valance band electrons. The behavior of these electrons mostly depends on the characteristics of their energy dispersion along the *k*-spaces directions such as Z-G-X-P-N-G within the Brillouin zone. In this study, the electronic energy dispersion graph at 0 and 8 GPa pressures along the highly symmetric directions of the Brillouin zone of $CaPd_2P_2$ are analyzed and depicted in Figure 3. The Fermi level ($E_F$) is displayed by the broken red line at zero of the photon energy scale. The overlap of the valance and conduction bands is observed at $E_F$ for both 0 and 8 GPa, indicating the metallic behavior of $CaPd_2P_2$.

To get a clear insight into the electronic properties of $CaPd_2P_2$, the total density of states (TDOS) and the partial density states (PDOS) are calculated. As shown in Figure 4a, the calculated TDOS at the 0 GPa pressure at $E_F$ is ~1.93 states/eV/f.u., which does not change significantly with the applied pressure. At 0 GPa, the calculated TDOS value at $E_F$ was observed to be ~1.94 states/eV/f.u. in the earlier study, which supports the present investigation.[25] As the band structure and the TDOS do not change significantly with the applied pressure, DOS is analyzed further at 0 and 8 GPa only.

For more theoretical insight, the DOS of individual atoms Ca, Pd, and P in the $CaPd_2P_2$ structure are observed, and depicted in Figure 4b. The Pd and P states are largely responsible for the emergence of DOS in the valance band near $E_F$. At 0 GPa, the DOS of Ca, Pd, and P at $E_F$ is ~0.41, ~0.75, and ~0.77 states/eV/f.u., respectively, which do not change significantly with the applied pressure. From this above observation, it is obvious that Pd and P atoms contribute most to the emergence of DOS at $E_F$. The valance band energy between −7.5 and −2.0 eV is significantly contributed by the Pd-4d states along with a significant contribution from the P-3p states.

The valance band near $E_F$ (−2.0 to 0 eV) is highly dominated by the hybridization between the Pd-4d and P-3p states. This analysis reveals that these electrons are largely responsible for the emergence of superconductivity in $CaPd_2P_2$, which is also observed in previous investigations.[24,25] It is generally known that the copper pairs are formed by electrons with energies near the $E_F$, in accordance with the Bardeen−Cooper−Schrieffer (BCS) theory.[75] Figure 3 reveals that the contributions of Pd-4d and P-3p states in the valence band and Pd-4p and P-3p states at the conduction band are dominant, which also supports the previous investigation.[24,25]

**3.6. Superconducting Properties.** $CaPd_2P_2$ possesses low-temperature superconductivity with experimental $T_c$ ~1.0 K[24] and theoretical $T_c$ of 0.33 K.[25] The $T_c$ can be estimated using the following McMillan equation[76]

$$T_c = \frac{\theta_D}{1.45}\exp\left[-\frac{1.04\,(1+\lambda)}{\lambda - \mu^*(1+0.62\lambda)}\right] \quad (8)$$

where $\mu^*$ and $\lambda$ are the Coulomb pseudopotential and electron−phonon coupling constant, respectively. The Coulomb pseudopotential can be calculated using the TDOS values at the Fermi level, $N(E_F)$, by the following equation[77−79]

$$\mu^* = 0.26\frac{N(E_F)}{1 + N(E_F)} \quad (9)$$

The values of $\mu^*$ in the range from 0.1 to 0.15 are considered physically reasonable.[24,80] From the above equation, it can be concluded that the value of $\mu^*$ does not change significantly with the applied pressure as the DOS at the Fermi level, $N(E_F)$, of $CaPd_2P_2$ remains almost invariant with the increasing pressure. The $\lambda$ can be defined as, $\lambda = N(E_F)\ V_{e\text{-}ph}$, where $V_{e\text{-}ph}$ is the electron−phonon interaction energy. As the $N(E_F)$ exhibits slight variation (Figure 5) with the increasing applied pressure. Therefore, in the present study, the variation in $\lambda$ depends on the possible effect on $V_{e\text{-}ph}$ with the applied pressure. From the McMillan equation, it is expected that for a fixed value of $\lambda$ of the $CaPd_2P_2$ compound, $T_c$ may increase with the applied pressure due to the increasing trend of $\theta_D$ with pressure. This is because $\theta_D$ is linearly associated with $T_c$.



https://doi.org/10.1021/acsomega.2c01088
ACS Omega 2022, 7, 21528−21536

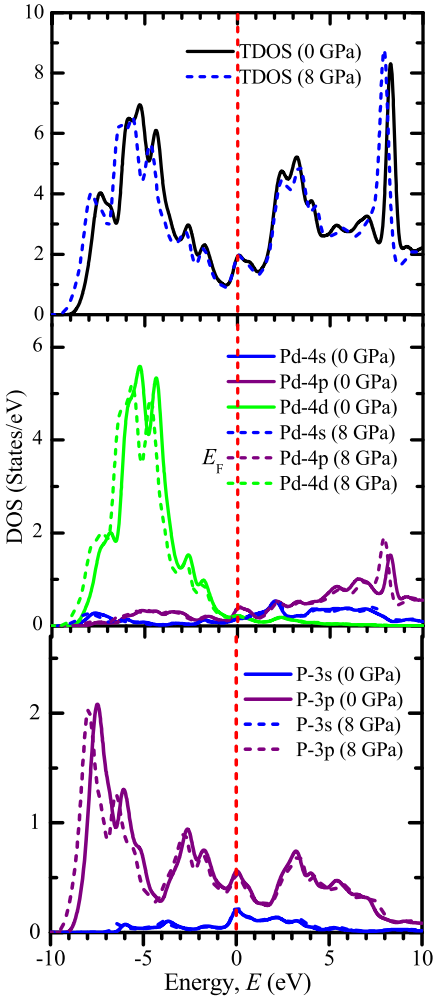


**Figure 5.** Calculated TDOS and PDOS (Pd, P) of $CaPd_2P_2$ under pressure.

## 4. CONCLUSIONS

First-principles DFT-based investigations have been carried out to study the structural, mechanical, thermophysical, optical, electronic, and superconducting properties of the $ThCr_2Si_2$-type tetragonal compound $CaPd_2P_2$ under pressure. The lattice parameters as well as the unit cell volume decrease with the applied pressure, which is the result of reducing space among the atoms with the increasing pressure. The elastic moduli show an increasing trend with the increasing pressure, which indicates that $CaPd_2P_2$ becomes increasingly stiff with the applied pressure. The study of Pugh's ratio and Poisson's ratio exhibits that $CaPd_2P_2$ has a ductile nature under the studied pressures. The study of universal anisotropy indices shows the significant anisotropic nature of $CaPd_2P_2$. The melting temperature increases with the applied pressure, which benefits the suitability of the higher-temperature applications of $CaPd_2P_2$. The $CaPd_2P_2$ compound reveals prominent optical absorption of UV radiation and becomes maximum near about 10 eV of photon energy. Almost a flat and significant amount of reflectivity is noticed between 9 and 18 eV of photon energy, and then the reflectivity spectra shift to the higher energy with the increasing applied pressure. The DOS analysis reveals that the Pd−P antibonding is largely responsible for the emergence of superconductivity in $CaPd_2P_2$, which justifies the previous reports. The value of DOS does not change significantly with the applied pressure. The increasing trend of the Debye temperature with pressure predicts that the superconducting transition temperature of the low-temperature superconductor $CaPd_2P_2$ might be increased with the applied pressure for a particular value of the electron−phonon coupling constant. This study concludes that applied pressure can be an efficient and clean thermodynamic approach to obtaining interesting physical properties of materials. The authors of this research work strongly believe that these interesting features of $CaPd_2P_2$ under pressure will attract enormous attention of the researchers to study the effects of pressure on superconducting materials both theoretically and experimentally.

## AUTHOR INFORMATION


### Corresponding Author

**Jakiul Islam** − *Department of Computer Science and Engineering, National Institute of Textile Engineering and Research, Dhaka 1350, Bangladesh; Department of Physics, Pabna University of Science and Technology, Pabna 6600, Bangladesh;* orcid.org/0000-0002-6113-5879; Email: jakiul.pust.phy.39@gmail.com

### Authors

**Nahida Farjana** − *Department of Physics, Pabna University of Science and Technology, Pabna 6600, Bangladesh*

**Md Didarul Islam** − *Department of Textile Engineering, National Institute of Textile Engineering and Research, Dhaka 1350, Bangladesh;* orcid.org/0000-0002-4663-6624

**Shamaita Shabnam** − *Department of Industrial and Production Engineering, National Institute of Textile Engineering and Research, Dhaka 1350, Bangladesh*

**Md Afjalur Rahman** − *Department of Physics, Pabna University of Science and Technology, Pabna 6600, Bangladesh*

Complete contact information is available at: https://pubs.acs.org/10.1021/acsomega.2c01088


### Notes

The authors declare no competing financial interest.

## REFERENCES


(1) Onnes, H. K.The Resistance of Pure Mercury at Helium Temperatures *Commun. Phys. Lab, Univ. Leiden*, 1911; Vol. *12*, p 120.

(2) Drozdov, A. P.; Eremets, M. I.; Troyan, I. A.; Ksenofontov, V.; Shylin, S. I. 2015. Conventional superconductivity at 203 kelvin at high pressures in the sulfur hydride system. *Nature* **2015**, *525*, 73−76.

(3) Troyan, I. A.; Semenok, D. V.; Kvashnin, A. G.; Sadakov, A. V.; Sobolevskiy, O. A.; Pudalov, V. M.; Ivanova, A. G.; Prakapenka, V. B.; Greenberg, E.; Gavriliuk, A. G.; Lyubutin, I. S. Anomalous high-temperature superconductivity in $YH_6$. *Adv. Mater.* **2021**, *33*, No. 2006832.

(4) Kong, P.; Minkov, V. S.; Kuzovnikov, M. A.; Drozdov, A. P.; Besedin, S. P.; Mozaffari, S.; Balicas, L.; Balakirev, F. F.; Prakapenka, V. B.; Chariton, S.; Knyazev, D. A. 2021. Superconductivity up to 243 K in the yttrium-hydrogen system under high pressure. *Nat. Commun.* **2021**, *12*, No. 5075.

(5) Snider, E.; Dasenbrock-Gammon, N.; McBride, R.; Debessai, M.; Vindana, H.; Vencatasamy, K.; Lawler, K. V.; Salamat, A.; Dias, R. P. Room-temperature superconductivity in a carbonaceous sulfur hydride. *Nature* **2020**, *586*, 373−377.

(6) Gor'kov, L. P.; Kresin, V. Z. Colloquium: High pressure and road to room temperature superconductivity. *Rev. Mod. Phys.* **2018**, *90*, No. 011001.

(7) Peng, F.; Sun, Y.; Pickard, C. J.; Needs, R. J.; Wu, Q.; Ma, Y. Hydrogen clathrate structures in rare earth hydrides at high pressures:




https://doi.org/10.1021/acsomega.2c01088
*ACS Omega* 2022, 7, 21528−21536

Possible route to room-temperature superconductivity. *Phys. Rev. Lett.* **2017**, *119*, No. 107001.
(8) Sukmas, W.; Tsuppayakorn-aek, P.; Pinsook, U.; Bovornratanaraks, T. Near-room-temperature superconductivity of Mg/Ca substituted metal hexahydride under pressure. *J. Alloys Compd.* **2020**, *849*, No. 156434.
(9) Wang, C.; Yi, S.; Cho, J. H. Multiband nature of room-temperature superconductivity in $LaH_{10}$ at high pressure. *Phys. Rev. B* **2020**, *101*, No. 104506.
(10) Hemley, R. J.; Ahart, M.; Liu, H.; Somayazulu, M. Road to room-temperature superconductivity: $T_c$ above 260 K in lanthanum superhydride under pressure, arXiv preprint arXiv:1906.03462, 2019.
(11) Verma, A. K.; Modak, P.; Schrodi, F.; Aperis, A.; Oppeneer, P. M. Phonon-mode specific contributions to room-temperature superconductivity in atomic hydrogen at high pressures. *Phy. Rev. B* **2019**, *103*, No. 094505.
(12) Wang, T.; Hirayama, M.; Nomoto, T.; Koretsune, T.; Arita, R.; Flores-Livas, J. A. Absence of conventional room-temperature superconductivity at high pressure in carbon-doped $H_3S$. *Phy. Rev. B* **2021**, *104*, No. 064510.
(13) Ge, Y.; Zhang, F.; Dias, R. P.; Hemley, R. J.; Yao, Y. Hole-doped room-temperature superconductivity in $H_3S_{1-x}Z_x$ (Z = C, Si). *Mater. Today Phys.* **2020**, *15*, No. 100330.
(14) Boeri, L.; Hennig, R. G.; Hirschfeld, P. J.; Profeta, G.; Sanna, A.; Zurek, E.; Pickett, W. E.; Amsler, M.; Dias, R.; Eremets, M.; Heil, C. The 2021 room-temperature superconductivity roadmap. *J. Condens. Matter Phys.* **2021**, *34*, No. 183002.
(15) Liu, L.; Wang, C.; Yi, S.; Kim, K. W.; Kim, J.; Cho, J. H. Microscopic mechanism of room-temperature superconductivity in compressed $LaH_{10}$. *Phy. Rev. B* **2019**, *99*, No. 140501.
(16) Esquinazi, P. D.; Precker, C. E.; Stiller, M.; Cordeiro, T. R.; Barzola-Quiquia, J.; Setzer, A.; Böhlmann, W. Evidence for room temperature superconductivity at graphite interfaces. *Quantum Stud.: Math. Found.* **2018**, *5*, 41−53.
(17) Szeftel, J.; Sandeau, N.; Abou Ghantous, M.; El-Saba, M. Towards room-temperature superconductivity. *Europhys. Lett.* **2021**, *134*, No. 27002.
(18) Pickett, W.; Eremets, M. The quest for room-temperature superconductivity in hydrides. *Phys. Today* **2019**, *72*, 52−58.
(19) Gubler, M.; Flores-Livas, J. A.; Kozhevnikov, A.; Goedecker, S. Missing theoretical evidence for conventional room-temperature superconductivity in low-enthalpy structures of carbonaceous sulfur hydrides. *Phys. Rev. Mater.* **2022**, *6*, No. 014801.
(20) Hirsch, J. E.; Marsiglio, F. Nonstandard superconductivity or no superconductivity in hydrides under high pressure. *Phy. Rev. B* **2021**, *103*, No. 134505.
(21) Hirsch, J. E.; Marsiglio, F. Absence of magnetic evidence for superconductivity in hydrides under high pressure. *Phys. C* **2021**, *584*, No. 1353866.
(22) Dogan, M.; Cohen, M. L. Anomalous behavior in high-pressure carbonaceous sulfur hydride. *Phys. C* **2021**, *583*, No. 1353851.
(23) Talantsev, E. F. The electron-phonon coupling constant, Fermi temperature and unconventional superconductivity in the carbonaceous sulfur hydride 190 K superconductor. *Supercond. Sci. Technol.* **2021**, *34*, No. 034001.
(24) Blawat, J.; Swatek, P. W.; Das, D.; Kaczorowski, D.; Jin, R.; Xie, W. Pd-P antibonding interactions in $APd_2P_2$ (A = Ca and Sr) superconductors. *Phys. Rev. Mater.* **2020**, *4*, No. 014801.
(25) Islam, J.; Hossain, A. A. Investigation of physical and superconducting properties of newly synthesized $CaPd_2P_2$ and $SrPd_2P_2$. *J. Alloys Compd.* **2021**, *868*, No. 159199.
(26) Banu, I. S.; Rajagopalan, M.; Yousuf, M.; Shenbagaraman, P. Electronic and bonding properties of $ANi_2P_2$ (A = Ca, Sr, Ba). *J. Alloys Compd.* **1999**, *288*, 88−95.
(27) Ban, Z.; Sikirica, M. The crystal structure of ternary silicides $ThM_2Si_2$(M = Cr, Mn, Fe, Co, Ni and Cu). *Acta Crystallogr.* **1965**, *18*, 594−599.
(28) Jeitschko, W.; Hofmann, W. K. Ternary alkaline earth and rare earth metal palladium phosphides with $ThCr_2Si_2$- and $La_6Ni_6P_{17}$-type structures. *J. Less Common Metals* **1983**, *95*, 317−322.
(29) Bauer, E. D.; Ronning, F.; Scott, B. L.; Thompson, J. D. Superconductivity in $SrNi_2As_2$. single crystals. *Phys. Rev. B* **2008**, *78*, No. 172504.
(30) Subedi, A.; Singh, D. J. Density functional study of $BaNi_2As_2$: electronic structure, phonons, and electron-phonon superconductivity. *Phys. Rev. B* **2008**, *78*, No. 132511.
(31) Ronning, F.; Klimczuk, T.; Bauer, E. D.; Volz, H.; Thompson, J. D. Synthesis and properties of $CaFe_2As_2$ single crystals. *J. Phys. Condens. Matter* **2008**, *20*, No. 322201.
(32) Basov, D. N.; Chubukov, A. V. Manifesto for a higher $T_c$. *Nat. Phys.* **2011**, *7*, 272−276.
(33) Uhoya, W. O.; Montgomery, J. M.; Tsoi, G. M.; Vohra, Y. K.; McGuire, M. A.; Sefat, A. S.; Sales, B. C.; Weir, S. T. Phase transition and superconductivity of $SrFe_2As_2$ under high pressure. *J. Phys. Condens. Matter* **2011**, *23*, No. 122201.
(34) Alireza, P. L.; Ko, Y. C.; Gillett, J.; Petrone, C. M.; Cole, J. M.; Lonzarich, G. G.; Sebastian, S. E. Superconductivity up to 29 K in SrFe2As2 and BaFe2As2 at high pressures. *J. Phys. Condens. Matter* **2009**, *21*, No. 012208.
(35) Miclea, C. F.; Nicklas, M.; Jeevan, H. S.; Kasinathan, D.; Hossain, Z.; Rosner, H.; Gegenwart, P.; Geibel, C.; Steglich, F. Evidence for a reentrant superconducting state in $EuFe_2As_2$ under pressure. *Phys. Rev. B* **2009**, *79*, No. 212509.
(36) Ronning, F.; Bauer, E. D.; Park, T.; Baek, S. H.; Sakai, H.; Thompson, J. D. Superconductivity and the effects of pressure and structure in single-crystalline $SrNi_2P_2$. *Phys. Rev. B* **2009**, *79*, No. 134507.
(37) Sefat, A. S.; Jin, R.; McGuire, M. A.; Sales, B. C.; Singh, D. J.; Mandrus, D. Superconductivity at 22 K in Co-doped $BaFe_2As_2$ crystals. *Phys. Rev. Lett.* **2008**, *101*, No. 117004.
(38) Shan, L.; Gong, J.; Wang, Y. L.; Shen, B.; Hou, X.; Ren, C.; Li, C.; Yang, H.; Wen, H. H.; Li, S.; Dai, P. Evidence of a spin resonance mode in the iron-based superconductor Ba0.6K0.4Fe2As2 from scanning tunneling spectroscopy. *Phys. Rev. Lett.* **2012**, *108*, No. 227002.
(39) Hirai, D.; von Rohr, F.; Cava, R. J. Emergence of superconductivity in $BaNi_2(Ge_{1-x}P_x)_2$ at a structural instability. *Phys. Rev. B* **2012**, *86*, No. 100505.
(40) Jeitschko, W.; Reehuis, M. Magnetic properties of $CaNi_2P_2$ and the corresponding lanthanoid nickel phosphides with $ThCr_2Si_2$ type structure. *J. Phys. Chem. Solids* **1987**, *48*, 667−673.
(41) An, J.; Sefat, A. S.; Singh, D. J.; Du, M. H. Electronic structure and magnetism in $BaMn_2As_2$ and $BaMn_2Sb_2$. *Phys. Rev. B* **2009**, *79*, No. 075120.
(42) Parvin, F.; Naqib, S. H. Pressure dependence of structural, elastic, electronic, thermodynamic, and optical properties of van der Waals-type $NaSn_2P_2$ pnictide superconductor: insights from DFT study. *Results Phys.* **2021**, *21*, No. 103848.
(43) Clark, S. J.; Segall, M. D.; Pickard, C. J.; Hasnip, P. J.; Probert, M. I. J.; Refson, K.; Payne, M. C. First principles methods using CASTEP. *Z. Kristallogr. - Cryst. Mater.* **2005**, *220*, 567−570.
(44) Hohenberg, P.; Kohn, W. Inhomogeneous electron gas. *Phys. Rev. B* **1964**, *136*, B864−B871.
(45) Kohn, W.; Sham, L. J. Self-consistent equations including exchange and correlation effects. *Phys. Rev. A* **1965**, *140*, 1133−1138.
(46) Perdew, J. P.; Burke, K.; Ernzerhof, M. Generalized gradient approximation made simple. *Phys. Rev. Lett.* **1996**, *77*, 3865−3868.
(47) Vanderbilt, D. Soft self-consistent pseudopotentials in a generalized eigenvalue formalism. *Phys. Rev. B* **1990**, *41*, 7892−7895.
(48) Monkhorst, H. J.; Pack, J. D. Special points for Brillouin-zone integration. *Phys. Rev. B* **1976**, *13*, 5188−5192.
(49) Fischer, T. H.; Almlof, J. General methods for geometry and wave function optimization. *J. Phys. Chem. A* **1992**, *96*, 9768−9774.
(50) Murnaghan, F. D. Finite deformations of an elastic solid. *Am. J. Math.* **1937**, *59*, 235−260.
(51) Born, M.; Huang, K. *Dynamical Theory of Crystal Lattices*; Oxford University Press: UK, 1998.


https://doi.org/10.1021/acsomega.2c01088
*ACS Omega* 2022, 7, 21528−21536

(52) Grimvall, G.; Magyari-Köpe, B.; Ozoliņš, V.; Persson, K. A. Lattice instabilities in metallic elements. *Rev. Mod. Phy.* **2012**, *84*, 945−986.
(53) Cleri, F.; Wang, J.; Yip, S. Lattice instability analysis of a prototype intermetallic system under stress. *J. Appl. Phys.* **1995**, *77*, 1449−1458.
(54) Mayengbam, R.; Tripathy, S. K.; Palai, G.; Dhar, S. S. 2018. First-principles study of phase transition, electronic, elastic and optical properties of defect chalcopyrite $ZnGa_2Te_4$ semiconductor under different pressures. *J. Phys. Chem. Solids* **2018**, *119*, 193−201.
(55) Voigt, W. Lehrbuch der Kristallphysik, Leipzig, Taubner *Adv. Earth Sci.*, 1928.
(56) Reuss, A. Berechnung der Fließgrenze von Mischkristallen auf Grund der Plastizitätsbedingung für Einkristalle. *Z. Angew. Math. Mech.* **1929**, *9*, 49−58.
(57) Hill, R. The elastic behaviour of a crystalline aggregate. *Proc. Phys. Soc. A* **1952**, *65*, 349−354.
(58) Islam, J.; Hossain, A. K. M. Narrowing band gap and enhanced visible-light absorption of metal-doped non-toxic $CsSnCl_3$ metal halides for potential optoelectronic applications. *RSC Adv.* **2020**, *10*, 7817−7827.
(59) Islam, J.; Hossain, A. K. M. Semiconducting to metallic transition with outstanding optoelectronic properties of $CsSnCl_3$ perovskite under pressure. *Sci. Rep.* **2020**, *10*, No. 14391.
(60) Islam, M. A.; Islam, J.; Islam, M. N.; Sen, S. K.; Hossain, A. A. Enhanced ductility and optoelectronic properties of environment-friendly $CsGeCl_3$ under pressure. *AIP Adv.* **2021**, *11*, No. 045014.
(61) Pugh, S. F. XCII. Relations between the elastic moduli and the plastic properties of polycrystalline pure metals. *London, Edinburgh, Dublin Philos. Mag. J. Sci.* **1954**, *45*, 823−843.
(62) Frantsevich, I. N.; Voronov, F. F.; Bokuta, S. A. *Elastic Constants and Elastic Moduli of Metals and Insulators Handbook*; Naukova Dumka: Kiev, 1983.
(63) Anderson, O. L.; Demarest, H. H., Jr. Elastic constants of the central force model for cubic structures: Polycrystalline aggregates and instabilities. *J. Geophys. Res.* **1971**, *76*, 1349−1369.
(64) Ranganathan, S. I.; Ostoja-Starzewski, M. Universal elastic anisotropy index. *Phys. Rev. Lett.* **2008**, *101*, No. 055504.
(65) Hadi, M. A.; Ali, M. S.; Naqib, S. H.; Islam, A. K. M. A. New ternary superconducting compound $LaRu_2As_2$: Physical properties from density functional theory calculations. *Chin. Phys. B* **2017**, *26*, No. 037103.
(66) Anderson, O. L. A simplified method for calculating the Debye temperature from elastic constants. *J. Phys. Chem. Solids* **1963**, *24*, 909−917.
(67) Wei, J. C.; Chen, H. C.; Huang, W.; Long, J. Theoretical investigation of the elastic, Vickers hardness and thermodynamic properties of $\delta$-WN under pressure. *Mater. Sci. Semicond. Process.* **2014**, *27*, 883−890.
(68) Zhou, S. Y.; Long, J. P.; Huang, W. Theoretical prediction of the fundamental properties of ternary bismuth tellurohalides. *Mater. Sci. Semicond. Process.* **2014**, *27*, 605−610.
(69) Long, J. P.; Yang, L. J.; Huang, W. Theoretical prediction of the fundamental properties for the ternary MgYZn and $Mg_{0.9}YZn_{1.06}$ alloys. *Comput. Mater. Sci.* **2014**, *91*, 315−319.
(70) Huang, W.; Chen, H. C. Investigation of the elastic, hardness, and thermodynamic properties of actinide oxides. *Phys. B: Condens. Matter* **2014**, *449*, 133−137.
(71) Rahaman, M. Z.; Rahman, M. A. Novel 122-type Ir-based superconductors $BaIr_2Mi_2$ (Mi = P and As): a density functional study. *J. Alloys Compd.* **2017**, *711*, 327−334.
(72) Kholil, M. I.; Bhuiyan, M. T. H. Electronic, elastic, vibrational and superconducting properties of a ternary superconductors LaIrP (P = P, As): insights from DFT. *Solid State Commun.* **2020**, *322*, No. 114053.
(73) Fine, M. E.; Brown, L. D.; Marcus, H. L. Elastic constants versus melting temperature in metals. *Scr. Metall.* **1984**, *18*, 951−956.
(74) Erum, N.; Iqbal, M. A. Effect of pressure variation on structural, elastic, mechanical, optoelectronic and thermodynamic properties of $SrNaF_3$ fluoroperovskite. *Mater. Res. Express* **2017**, *4*, No. 126311.
(75) Karaca, E.; Tütüncü, H. M.; Uzunok, H. Y.; Srivastava, G. P.; Uğur, S. Theoretical investigation of superconductivity in $SrPd_2Ge_2$, $SrPd_2As_2$, and $CaPd_2As_2$. *Phys. Rev. B* **2016**, *93*, No. 054506.
(76) McMillan, W. L. Transition temperature of strong-coupled superconductors. *Phys. Rev.* **1968**, *167*, 331−344.
(77) Kholil, M. I.; Ali, M. S.; Aftabuzzaman, M. Structural, elastic, electronic and vibrational properties of $BaRh_2P_2$ and $SrIr_2As_2$ superconductors: a DFT study. *J. Alloys Compd.* **2018**, *740*, 754−765.
(78) Khan, N. S.; Rano, B. R.; Syed, I. M.; Islam, R. S.; Naqib, S. H. First-principles prediction of pressure dependent mechanical, electronic, optical, and superconducting state properties of $NaC_6$: A potential high-Tc superconductor. *Results Phys.* **2022**, *33*, No. 105182.
(79) *Superconductivity in d- and f-Band Metals*; Douglass, D., Ed.; Springer: US, 1976.
(80) Islam, J.; Rahman, M. A.; Hossain, A. A. Physical and Superconducting Properties of Chiral Noncentrosymmetric $TaRh_2B_2$ and $NbRh_2B_2$: A Comprehensive DFT Study. *ACS Appl. Electron. Mater.* **2022**, *4*, 1143−1152.


https://doi.org/10.1021/acsomega.2c01088
*ACS Omega* 2022, 7, 21528−21536